Mechanical Systems and Signal Processing 123 (2019) 68–83

Contents lists available at ScienceDirect

Mechanical Systems and Signal Processing

journal homepage: www.elsevier.com/locate/ymssp

Accounting for amplitude of excitation in model updating through a hierarchical Bayesian approach: Application to a two-story reinforced concrete building

Mingming Song [a], Babak Moaveni [a,*], Costas Papadimitriou [b], Andreas Stavridis [c]

[a] Dept. of Civil and Environmental Engineering, Tufts University, Medford, MA, USA
[b] Dept. of Mechanical Engineering, University of Thessaly, Volos, Greece
[c] Dept. of Civil, Structural and Environmental Engineering, University at Buffalo, NY, USA

ARTICLE INFO

Article history:
Received 10 August 2018
Received in revised form 10 November 2018
Accepted 21 December 2018

Keywords:
Hierarchical Bayesian model updating
Structural identification
Effects of excitation level
Response prediction
Modeling errors
Reinforced concrete building

ABSTRACT

Calibrated linear equivalent models of civil structures are often used for response prediction and performance assessment. However, these models are only valid for a narrow range of excitation level for which these models are calibrated. In this paper a hierarchical Bayesian model updating approach is proposed for model calibration and response prediction of dynamic structural systems in a wide range of excitation levels where the linear equivalent stiffness of different structural components are updated as functions of excitation amplitude. The proposed approach is implemented on a two-story reinforced concrete building with masonry infills. The building, located in El Centro California, has suffered severe damage during past earthquakes. Ambient and forced vibration tests were performed on the building using an eccentric mass shaker, and its dynamic response was measured using an array of accelerometers. The modal parameters of the structure are identified under different amplitudes of vibration and the natural frequencies exhibit significant decrease at higher vibration levels. The hierarchical Bayesian model updating approach is used to estimate the probability distribution of effective stiffness of considered structural components which is characterized by the stiffness mean and covariance as hyperparameters, as well as modeling errors. To account for the effect of vibration amplitude, the effective stiffness mean is considered as a function of vibration level. A two-step sampling approach is proposed to evaluate the joint posterior probability distribution of updating parameters. The calibrated model is then used to predict time history response of the building under forced vibration which is compared with measured data. The good agreement observed from this comparison verifies the calibrated model and the proposed approach to account for the excitation level in updating process.

1. Introduction

Model updating, also referred to as model inversion or model calibration, has been widely used for structural health or performance assessment, and response prediction of dynamic systems [1,2]. In the application of model updating, model parameters are updated to minimize an objective function which is the misfit between model-predicted and measured data

* Corresponding author.
E-mail address: babak.moaveni@tufts.edu (B. Moaveni).

https://doi.org/10.1016/j.ymssp.2018.12.049
0888-3270/

features. Finite element (FE) model updating has the advantage of integrating field measurements with a physics-based FE model to provide an accurate representation of the actual structure system. The calibrated model can then be used for response prediction and/or damage detection. Applications of model updating for assessment of complex real-world civil structures include mainly bridges [3–11] and buildings [12–16]. Teughels and Roeck [6] performed damage identification of a prestressed concrete bridge through model updating. Reynders et al. [9] applied model updating for damage identification of a bridge using modal strains measured directly by optical fiber strain sensors. Jaishi et al. [7] presented FE model updating of a concrete-filled tubular arch bridge using modal flexibility. Song et al. [15] implemented FE model updating for damage identification of the two-story RC building (the same building considered in this study) and compared the results with lidar measurement. Bassoli et al. [16] performed model updating of a damaged masonry tower using ambient vibration measurements.

The deterministic applications of model updating, however, cannot justify the uncertainty of updating results. The model updating results depend on a variety of factors such as the completeness and accuracy of measurements, the number of sensors used, and the modeling assumptions (i.e., modeling errors). Among these factors, modeling errors provide the biggest challenge in utilizing calibrated models for structural response prediction, especially outside their calibration domain [13,14,17]. Bayesian model updating approaches have been used to account for different sources of modeling errors when dealing with real-world structural systems [18–20]. The numerical applications of the Bayesian approach to the IASC-ASCE benchmark are reported in these two studies [21,22]. Muto and Beck [23] employed Bayesian model updating and model class selection for a numerical 3-story shear building. Ntotsios et al. [24] performed Bayesian damage identification of a laboratory small-scaled bridge section. Lam et al. [25] applied a Bayesian approach for model updating and damage detection of a 2-story steel frame in the laboratory. Behmanesh and Moaveni [26] implemented Bayesian model updating to identify simulated damage (added concrete block on the deck) on a footbridge, and considered the effect of temperature and excitation amplitude using hierarchical Bayesian approach [27].

Although the Bayesian model updating applications quantify the uncertainty of updating results, the obtained uncertainties reflect only the estimation errors and become negligible (go to zero) with increasing amount of (even noisy) data. Such approaches cannot quantify the variability of effective modeling parameter due to ambient and environmental conditions such as changing temperature, humidity, wind, or traffic loading. In these studies [13,14], the authors have reported that the accuracy of model predictions would vary significantly with excitation amplitude for linear dynamic models. Structures are assumed to respond as quasi-linear systems with their dynamic parameters evolving as a function of structural damage and excitation amplitude. With increasing levels of excitation, the level of nonlinearity in the structural response increases, even at relatively low amplitude excitations. Therefore, the assumption that the structure behaves as a quasi-linear dynamic system is violated and a linear dynamic model (e.g., modal model) is not strictly able to represent the structure accurately at different levels of excitation. A nonlinear model updating approach could be potentially applied to solve this issue as reported in Asgarieh et al. [28], but this requires measurements at full range of nonlinear response and complex material models capable of representing actual nonlinear behavior.

In this study, we propose a hierarchical Bayesian model updating approach where the effective stiffness parameters are assumed to be functions of excitation amplitude. The approach is implemented for model updating and response prediction of a two-story reinforced concrete (RC) building which was tested using an eccentric mass shaker. The hierarchical Bayesian approach [29] is implemented to estimate the effective stiffness of the considered structural components and parameters which characterize their probability distributions including the mean and covariance as hyperparameters, as well as modeling errors. To account for the effect of vibration amplitude, the stiffness mean is considered as a function of vibration level. The joint posterior probability distribution of all updating parameters (effective stiffness, stiffness mean which is a function of vibration level, stiffness covariance, and modeling errors) is derived from likelihood functions and prior probability distributions. A two-step sampling approach is proposed to evaluate the posterior distribution by computing the most probable values of parameters at the first step, and then using Gibbs sampler to generate parameter samples. The calibrated model is shown to be capable of capturing the decreasing trend of identified natural frequencies and predicting the building response to shaker excitation accurately.

2. Dynamic test of the structure

The considered structure is a two-story RC building with masonry walls, located in El Centro, California. It consists of RC frames in north–south direction and peripheral masonry infills on both stories, with a small wooden extension on the south side. The building was severely damaged by four significant earthquakes and has been abandoned, as it is considered not economy-efficient for reparation and reuse. Fig. 1 shows the north-east and south-west views of the structure. Dominant shear cracks were observed in the masonry walls and concrete columns of the second story. This building provided a unique opportunity to perform a set of dynamic tests under significant excitation levels on a real-world RC structure. Ambient and forced vibration tests were performed and the structural response was measured through an array of accelerometers in the building. A total of 15 tri-axial accelerometers were installed with 5 accelerometers on each floor (1st floor, 2nd floor and roof). The layout of accelerometers on each floor is similar, with the 2nd floor layout demonstrated in Fig. 2(a). The acronyms NW, NE, SW, SE and CC refer to north-west, north-east, south-west, south-east and center. The positive X, Y and Z axis of the tri-axial accelerometer are pointing to the east, north and upward direction, respectively. In this study, only the horizontal

Fig. 1. (a) North-east view and (b) south-west view of the structure [30].

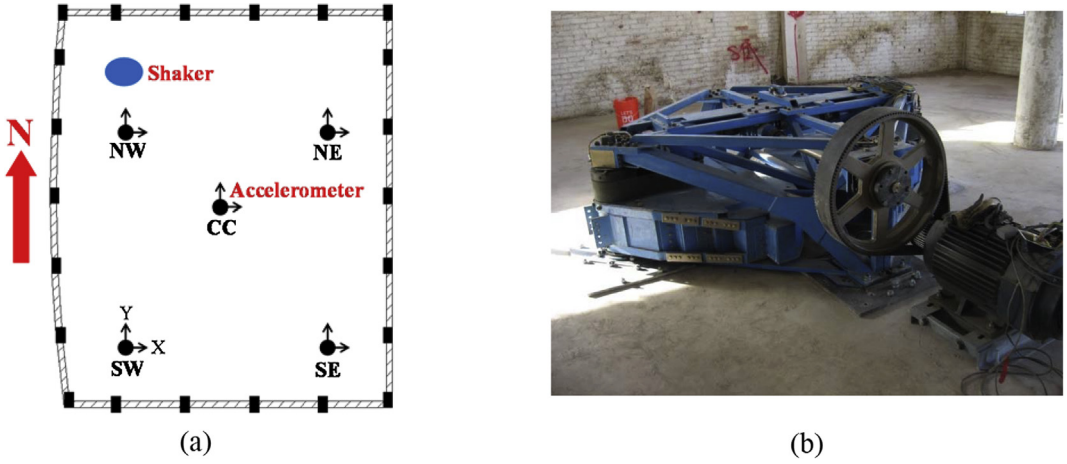

Fig. 2. (a) Layout of accelerometers on the 2nd floor; (b) The eccentric mass shaker [30].

components (X and Y) of measured accelerations are used in system identification, resulting in a total of 30 channels. The forced vibration tests were done using a uniaxial eccentric mass shaker located at the north-west corner of the 2nd floor, as depicted in Fig. 2. Multiple different forced excitations were performed on the building, with the excitation either in sine sweep or sine step form and the shaking direction either in north-south or east-west direction. In total, 300 min of ambient vibration data were recorded, and 11 forced vibration tests (each between 3 and 6 min long) were performed. More details about the instrumentations and dynamic test of the structure can be found in these studies [15,30].

3. System identification under different excitation levels

System identification is performed to extract the modal parameters (natural frequencies, mode shapes and damping ratios) of the building using both ambient and forced vibration data. For ambient vibration, the measured acceleration data are divided into 10-min long windows, and the Natural Excitation Technique [31] combined with Eigensystem Realization Algorithm [32] (NExT-ERA) is used to estimate the modal parameters of the structure, resulting in a total of 30 datasets. Fig. 3 (a) shows a sample stabilization diagram and the power spectral density of SW-X channel on the roof for an ambient vibration dataset. For forced vibration, peak-picking in frequency-domain is employed to estimate the modal parameters using the estimated transfer functions between different measurement channels and a reference channel [33]. The transfer functions are estimated as the ratio of the cross-power spectral density of different acceleration channels with the reference channel to the auto-power spectral density of the reference channel. The reference channel is selected as the channel of the NW accelerometer on the 2nd floor in the same direction as the shaker excitation (X or Y). Fig. 3(b) shows a sample transfer function between the NW-Y channel on the roof and the reference channel NW-Y on the 2nd floor for a forced vibration test in Y direction. A total of 41 sets (30 from ambient vibration data and 11 from forced vibration data) of modal parameters are identified and their statistics are reported in Table 1 for the first two modes. The corresponding two mode shapes are shown in Fig. 4. Note that the average mode shapes are plotted here, which are defined as the arithmetic mean of all the normalized mode shapes estimated from ambient vibration data. It can be seen that both modes include translational and torsional movement, with mode 1 having larger motion in the X direction (west-east) and mode 2 in Y direction

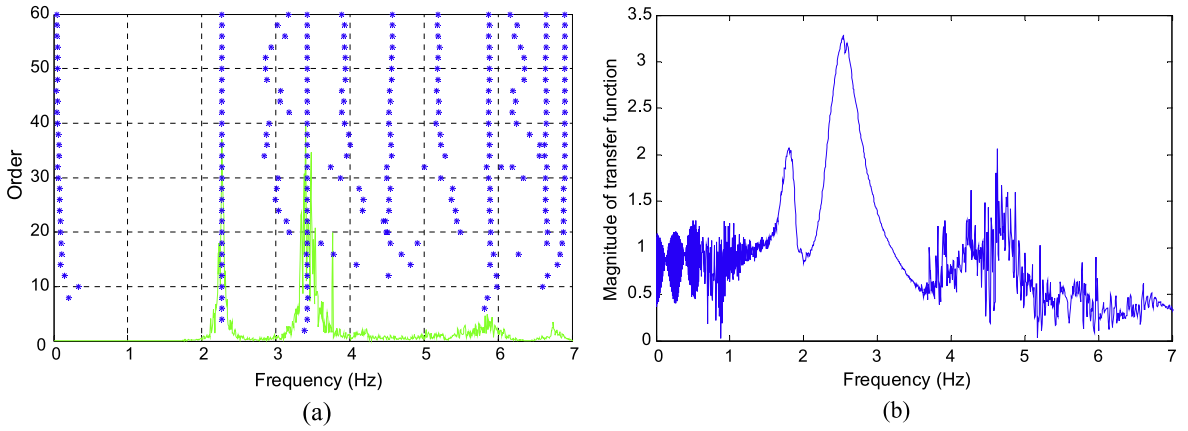

Fig. 3. (a) Stabilization diagram and power spectral density of SW-X channel on roof for ambient vibration data; (b) Sample transfer function between NW-Y channel on the roof and NW-Y channel on 2nd floor for a forced vibration test.

Table 1
The statistics summary of the identified modal parameters.

		Natural frequency (Hz)		MAC		Damping ratio (%)	
		Mode 1	Mode 2	Mode 1	Mode 2	Mode 1	Mode 2
Ambient (n = 30)	Mean	2.26	3.37	1.00	1.00	1.5	2.5
	Std	0.01	0.04	0.002	0.002	0.3	0.4
Forced (n = 11)	Mean	1.77	2.41	0.97	0.96	5.9	8.6
	Std	0.10	0.16	0.019	0.011	1.1	1.2

Note: Std denotes standard deviation.

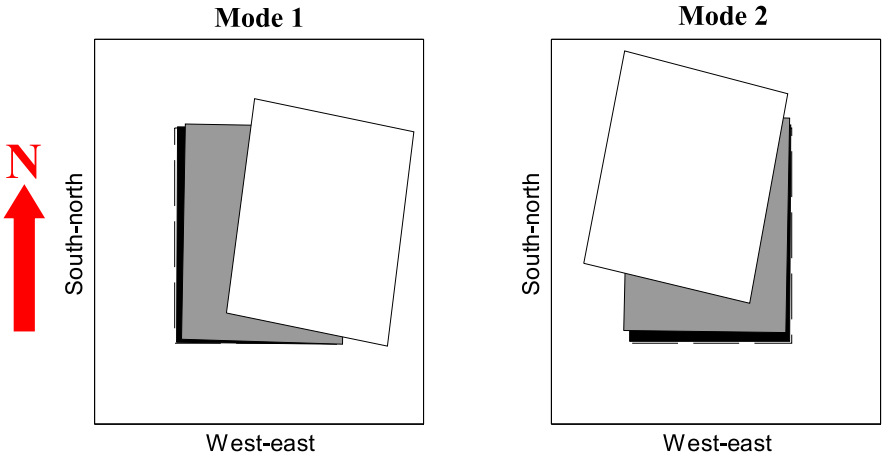

Fig. 4. Mode shapes of identified modes 1 and 2 (white, grey and black indicate roof, 2nd floor and 1st floor, respectively, and dashed rectangle presents the undeformed floor positions).

(south-north). The motion of first floor is negligible, the second floor has small motion, and the roof moves significantly larger than the lower floors for both vibration modes. This is due to the smaller lateral stiffness of the second story compared to the first story. When using forced vibration data, the mode shape of mode 1 is identified more accurately when the shaker excitation is in X direction, and similarly mode 2 is more accurately identified with shaker excitation in Y direction. This is due to the interaction of modal response in one direction and the strong shaker excitation force in the other direction, and has been reported in the thesis [30]. In this study, to keep a complete set of modal parameters (i.e., no missed identification), the missing or less accurately identified mode shapes are replaced by the identified mode shapes with higher accuracy at the closest vibration amplitude from other datasets. It is worth noting that while the natural frequencies show significant sensitivity with respect to excitation amplitude, the variability of mode shapes is small.

In Table 1, the reported modal assurance criterion (MAC) values are between the identified mode shapes and the average mode shapes from ambient vibration data. It can be observed that the identified natural frequencies of both modes show a significant drop between ambient and forced vibrations, which is much larger than the observed uncertainties in each type of excitation as already reported in the study [30]. However, the identified mode shapes from ambient and forced vibrations are very similar. An evident increase of the identified damping ratios for both modes can be seen from ambient to forced vibration. The decreasing trend of the natural frequencies can be observed in Fig. 5, in which the natural frequencies are plotted against the vibration level of the structure. The vibration level is defined as the average of the root mean square (RMS) of the acceleration time history measured by NW accelerometer on the roof in X and Y directions. This definition of the vibration level is to represent overall vibration amplitude of the structure. From Fig. 5, it can be seen that the natural frequencies from ambient vibration data are clustered together close to the vertical axis due to the small vibration amplitude (∼1e-4). The vibration levels for forced excitation tests are significantly larger due to the large capacity of the shaker (444.8 kN). Different excitation forces are achieved by changing the mass setup of the shaker shaft and the input frequency. It can be seen that a proximate linear relationship can be observed between natural frequencies and vibration levels, as denoted by the dashed line in Fig. 5. The decreasing trend of natural frequencies with higher vibration level can be attributed to crack opening in concrete and masonry with larger vibration amplitude. It is worth noting that this drop in natural frequencies is not permanent (i.e., not due to damage) and is recovered after the shaker tests as the identified natural frequencies from ambient vibration data roughly remain unchanged before and after the shaking test, as reported by Yousefianmoghadam [30]. This stiffness-amplitude dependence phenomenon has been observed and reported in several other studies [13,27,34].

4. Hierarchical Bayesian model updating

4.1. Formulation of updating framework with amplitude dependent parameters

Based on Fig. 5, the identified natural frequencies of both modes appear to follow a linear decreasing relationship with the vibration level, which inspires the idea of formulating a stiffness-amplitude relationship within the hierarchical Bayesian model updating. In this formulation, the stiffness of different structural components are considered as the updating stiffness parameters $\boldsymbol{\theta}$. The stiffness parameters are assumed to follow a normal distribution with their mean being a linear function of vibration level and covariance matrix being constant, $\boldsymbol{\theta} \sim N(\boldsymbol{\mu}_{\boldsymbol{\theta}}, \boldsymbol{\Sigma}_{\boldsymbol{\theta}})$, since no significant change is observed for the variation of natural frequencies at different vibration levels. The mean and covariance of stiffness parameters ($\boldsymbol{\mu}_{\boldsymbol{\theta}}$ and $\boldsymbol{\Sigma}_{\boldsymbol{\theta}}$) are called stiffness hyperparameters. Based on the assumption, the mean and covariance matrix can be expressed as

$$\boldsymbol{\mu}_{\boldsymbol{\theta}}(\varepsilon_t) = \mathbf{a} + \mathbf{b}\varepsilon_t \tag{1}$$

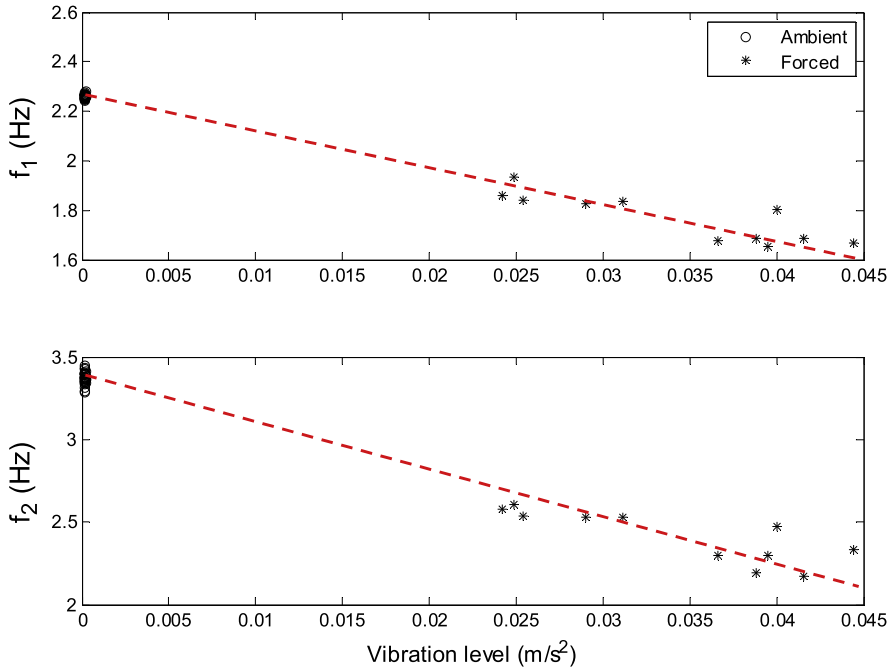

Fig. 5. Identified natural frequencies versus the vibration level.

$$\boldsymbol{\Sigma}_{\boldsymbol{\theta}} = \begin{bmatrix} \ddots & & \\ & \sigma_{\theta_i}^2 & \\ & & \ddots \end{bmatrix} \tag{2}$$

where vectors **a** and **b** represent the intercept and slope of the linear function. ε_t is the vibration level during test t. The covariance matrix $\boldsymbol{\Sigma}_{\boldsymbol{\theta}}$ is assumed to be a diagonal matrix, i.e., the stiffness parameters are assumed to be independent. This is a simplified and reasonable assumption if no evident correlation is observed between different structural components. Note that the full covariance matrix can also be updated in this framework which would add to the computation burden.

Error function $\mathbf{e}_t$ is defined as the difference between the model-predicted modal parameters and their identified counterparts, and is assumed to follow a zero-mean normal distribution $N(\mathbf{0}, \boldsymbol{\Sigma}_{\mathbf{e}})$, as shown in Eq. (3):

$$\mathbf{e}_t = \begin{bmatrix} \mathbf{e}_{\lambda_t} \\ \mathbf{e}_{\boldsymbol{\Phi}_t} \end{bmatrix} \sim N(\mathbf{0}, \boldsymbol{\Sigma}_{\mathbf{e}}) \tag{3}$$

where $\mathbf{e}_{\lambda_t}$ and $\mathbf{e}_{\boldsymbol{\Phi}_t}$ refer to eigen-frequency error and mode shape error, and are defined as

$$e_{\lambda_{tm}} = \frac{\tilde{\lambda}_{tm} - \lambda_m(\boldsymbol{\theta}_t)}{\lambda_m(\boldsymbol{\theta}_t)} \tag{4}$$

$$\mathbf{e}_{\boldsymbol{\Phi}_{tm}} = \frac{\tilde{\boldsymbol{\Phi}}_{tm}}{\|\tilde{\boldsymbol{\Phi}}_{tm}\|} - a_{tm} \frac{\boldsymbol{\Gamma}\boldsymbol{\Phi}_m(\boldsymbol{\theta}_t)}{\|\boldsymbol{\Gamma}\boldsymbol{\Phi}_m(\boldsymbol{\theta}_t)\|} \tag{5}$$

where $\boldsymbol{\theta}_t$ refers to the stiffness parameters during test t, and subscript m denotes the mode number. $\tilde{\lambda}_{tm} = (2\pi\tilde{f}_{tm})^2$ is the identified eigen-frequency and $\tilde{f}_{tm}$ is the identified natural frequency in Hz. $\tilde{\boldsymbol{\Phi}}_{tm}$ refers to the identified mode shape in dataset t, while $\lambda_m(\boldsymbol{\theta}_t)$ and $\boldsymbol{\Phi}_m(\boldsymbol{\theta}_t)$ are the model-predicted eigen-frequency and mode shape. $\boldsymbol{\Gamma}$ is the matrix that maps the corresponding components of $\boldsymbol{\Phi}_m(\boldsymbol{\theta}_t)$ with $\tilde{\boldsymbol{\Phi}}_{tm}$. a_{tm} is a scaling factor and defined as Eq. (6):

$$a_{tm} = \frac{\tilde{\boldsymbol{\Phi}}_{tm}^T \boldsymbol{\Gamma}\boldsymbol{\Phi}_m(\boldsymbol{\theta}_t)}{\|\tilde{\boldsymbol{\Phi}}_{tm}\| \|\boldsymbol{\Gamma}\boldsymbol{\Phi}_m(\boldsymbol{\theta}_t)\|} \tag{6}$$

Note that the definition of mode shape error in Eq. (5) is adopted from Beck et al. [35] which represents projection of model-predicted mode shape in the direction of measured mode shape. The mode shape error in Eq. (5) has been normalized to the length of the identified mode shape $\tilde{\boldsymbol{\Phi}}_{tm}$, providing comparable weights on different mode shape errors.

In this study, the effect of modeling errors and measurement noise is quantified approximately by fitting a normal distribution to the error function $\mathbf{e}_t$. Note that the mean of the error function $\boldsymbol{\mu}_{\mathbf{e}}$ is assumed to be zero in this study, i.e., no modeling bias is considered. However, if strong modeling bias is observed in the updated model, a non-zero $\boldsymbol{\mu}_{\mathbf{e}}$ can be considered as presented in the study [36]. The covariance of the error function $\boldsymbol{\Sigma}_{\mathbf{e}}$ is assumed to be a diagonal matrix by ignoring the correlations between different error function components (similar to $\boldsymbol{\Sigma}_{\boldsymbol{\theta}}$, the full matrix $\boldsymbol{\Sigma}_{\mathbf{e}}$ can also be potentially estimated), as written in Eq. (7):

$$\boldsymbol{\Sigma}_{\mathbf{e}} = \begin{bmatrix} \ddots & & \\ & \sigma_{e_j}^2 & \\ & & \ddots \end{bmatrix} \tag{7}$$

Note that the assumption of a diagonal $\boldsymbol{\Sigma}_{\mathbf{e}}$ is realistic for many applications, however, in case that correlation exists among error function components, the proposed hierarchical Bayesian approach is capable of estimating the full matrix $\boldsymbol{\Sigma}_{\mathbf{e}}$ which would follow the similar formulation with an inverse Wishart prior distribution used. However, this would add to the com-

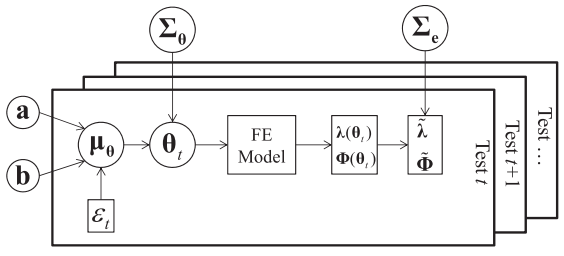

Fig. 6. Representation of the proposed hierarchical Bayesian framework.

putation burden by increasing the number of updating parameters. In the current study, since the estimated values of $\boldsymbol{\Sigma}_{\mathbf{e}}$ are relatively small, the influence of updating off-diagonal components of the error covariance matrix is expected to be small.

A diagram of the proposed hierarchical Bayesian framework is depicted in Fig. 6. Unlike the traditional Bayesian approach which usually only estimates the structural stiffness, the hierarchical Bayesian framework estimates parameters of the probability distribution of stiffness ($\mathbf{a}$, $\mathbf{b}$ and $\boldsymbol{\Sigma}_{\boldsymbol{\theta}}$) as hyperparameters, as well as covariance of error function $\boldsymbol{\Sigma}_{\mathbf{e}}$. Based on the Bayes' theorem, posterior probability density function (PDF) of all updating parameters is proportional to the product of likelihood function and prior PDFs [37]:

$$\begin{aligned} &p\left(\boldsymbol{\Theta}, \mathbf{a}, \mathbf{b}, \boldsymbol{\Sigma}_{\boldsymbol{\theta}}, \boldsymbol{\Sigma}_{\mathbf{e}} \middle| \tilde{\boldsymbol{\lambda}}, \tilde{\boldsymbol{\Phi}}, \boldsymbol{\varepsilon}\right) \\ &\propto \prod_{t=1}^{N_t} p\left(\tilde{\boldsymbol{\lambda}}_t, \tilde{\boldsymbol{\Phi}}_t | \boldsymbol{\theta}_t, \mathbf{a}, \mathbf{b}, \boldsymbol{\Sigma}_{\boldsymbol{\theta}}, \boldsymbol{\Sigma}_{\mathbf{e}}, \varepsilon_t\right) p(\boldsymbol{\theta}_t, \mathbf{a}, \mathbf{b}, \boldsymbol{\Sigma}_{\boldsymbol{\theta}}, \boldsymbol{\Sigma}_{\mathbf{e}} | \varepsilon_t) \\ &\propto \prod_{t=1}^{N_t} p\left(\tilde{\boldsymbol{\lambda}}_t, \tilde{\boldsymbol{\Phi}}_t | \boldsymbol{\theta}_t, \boldsymbol{\Sigma}_{\mathbf{e}}\right) p(\boldsymbol{\theta}_t | \mathbf{a}, \mathbf{b}, \boldsymbol{\Sigma}_{\boldsymbol{\theta}}, \varepsilon_t) p(\mathbf{a}) p(\mathbf{b}) p(\boldsymbol{\Sigma}_{\boldsymbol{\theta}}) p(\boldsymbol{\Sigma}_{\mathbf{e}}) \end{aligned} \tag{8}$$

in which, $\boldsymbol{\Theta}$, $\tilde{\boldsymbol{\lambda}}$, $\tilde{\boldsymbol{\Phi}}$ and $\boldsymbol{\varepsilon}$ denote the collections of stiffness vectors, identified eigen-frequencies, mode shapes and vibration levels of all datasets available, respectively. N_t is the total number of datasets, which is equal to 41 as mentioned previously. The prior PDFs of $\mathbf{a}$, $\mathbf{b}$, $\boldsymbol{\Sigma}_{\boldsymbol{\theta}}$ and $\boldsymbol{\Sigma}_{\mathbf{e}}$ are assumed to be independent. Uniform distributions are used for $\mathbf{a}$ and $\mathbf{b}$, and inverse $-\chi^2$ distributions are chosen for $\sigma^2_{\theta_i}$ and $\sigma^2_{e_j}$, as written below:

$$p(\mathbf{a}) \propto 1 \tag{9}$$

$$p(\mathbf{b}) \propto 1 \tag{10}$$

$$\sigma^2_{\theta_i} \sim \text{ Inverse} - \chi^2(\nu_1, \sigma^2_{\theta 0_i}) \tag{11}$$

$$\sigma^2_{e_j} \sim \text{ Inverse} - \chi^2(\nu_2, \sigma^2_{e 0_j}) \tag{12}$$

in which, $\nu_1, \sigma^2_{\theta 0_i}$, $\nu_2, \sigma^2_{e 0_j}$ are parameters of the prior distributions. It is advised to choose and tune these parameters based on specific applications as they can influence the posterior PDF. However, this influence will be reduced if more datasets are used in the updating process. In this study, the following values are used after the tuning process: $\nu_1 = 1$, $\sigma^2_{\theta 0_i} = 0.05^2$, $\nu_2 = 1$ and $\sigma^2_{e 0_j} = 1\text{e} - 6$. These prior PDFs are considered "conjugate priors", and will simplify the mathematical derivation of the joint posterior distribution [37].

After substituting the prior PDFs and the assumed likelihood functions into Eq. (8), the joint posterior distribution can then be derived as:

$$\begin{aligned} &p\left(\boldsymbol{\Theta}, \mathbf{a}, \mathbf{b}, \boldsymbol{\Sigma}_{\boldsymbol{\theta}}, \boldsymbol{\Sigma}_{\mathbf{e}} \middle| \tilde{\boldsymbol{\lambda}}, \tilde{\boldsymbol{\Phi}}, \boldsymbol{\varepsilon}\right) \\ &\propto |\boldsymbol{\Sigma}_{\boldsymbol{\theta}}|^{-\frac{N_t+\nu_1+2}{2}} |\boldsymbol{\Sigma}_{\mathbf{e}}|^{-\frac{N_t+\nu_2+2}{2}} \exp\left[\sum_{t=1}^{N_t}\left(-J_{\mathbf{e}_t} - J_{\boldsymbol{\theta}_t}\right) - \sum_{i=1}^{N_p} \frac{\nu_1 \sigma^2_{\theta 0_i}}{2\sigma^2_{\theta_i}} - \sum_{j=1}^{N_e} \frac{\nu_2 \sigma^2_{e 0_j}}{2\sigma^2_{e_j}}\right] \end{aligned} \tag{13}$$

$$J_{\mathbf{e}_t} = \frac{1}{2} \mathbf{e}_t^T \boldsymbol{\Sigma}_{\mathbf{e}}^{-1} \mathbf{e}_t \tag{14}$$

$$J_{\boldsymbol{\theta}_t} = \frac{1}{2} (\boldsymbol{\theta}_t - \mathbf{a} - \mathbf{b}\varepsilon_t)^T \boldsymbol{\Sigma}_{\boldsymbol{\theta}}^{-1} (\boldsymbol{\theta}_t - \mathbf{a} - \mathbf{b}\varepsilon_t) \tag{15}$$

where N_p denotes the number of stiffness components in $\boldsymbol{\theta}_t$, N_e is the dimension of error function $\mathbf{e}_t$ and equal to $(1 + N_s)N_m$, and N_m and N_s are number of identified modes and number of components in the identified mode shapes (number of sensors), respectively.

4.2. A two-step sampling approach to evaluate joint posterior distribution

The derived joint posterior PDF in Eq. (13) is only known up to a normalizing constant and is prohibitively difficult to solve analytically. The stochastic sampling method, Gibbs sampler [38], has been shown to be efficient to evaluate Eq. (13) numerically. Gibbs sampler requires the derivation of the conditional posterior PDFs for each of the updating parameters, which have been derived and presented below:

$$p(\boldsymbol{\theta}_t | \cdot) \propto \exp(-J_{\mathbf{e}_t} - J_{\boldsymbol{\theta}_t}) \tag{16}$$

$$p(\mathbf{a}|\cdot) = N\left(\frac{1}{N_t}\sum_{t=1}^{N_t}(\boldsymbol{\theta}_t - \mathbf{b}\varepsilon_t), \frac{1}{N_t}\boldsymbol{\Sigma}_{\boldsymbol{\theta}}\right) \tag{17}$$

$$p(\mathbf{b}|\cdot) \propto \exp\left(-\sum_{t}^{N_t} J_{\boldsymbol{\theta}_t}\right) \tag{18}$$

$$p(\sigma_{\theta_i}^2|\cdot) = \text{Inverse} - \chi^2\left(\nu_1 + N_t, \frac{\nu_1\sigma_{\theta 0_i}^2 + N_t S_i}{\nu_1 + N_t}\right) \tag{19}$$

$$p(\sigma_{e_j}^2|\cdot) = \text{Inverse} - \chi^2\left(\nu_2 + N_t, \frac{\nu_2\sigma_{e0_j}^2 + N_t V_j}{\nu_2 + N_t}\right) \tag{20}$$

$$S_i = \frac{1}{N_t}\sum_{t=1}^{N_t}(\theta_{t_i} - a_i - b_i\varepsilon_t)^2 \tag{21}$$

$$V_j = \frac{1}{N_t}\sum_{t=1}^{N_t} e_{t_j}^2 \tag{22}$$

in $p(\boldsymbol{\theta}_t|\cdot)$ which denotes the conditional posterior PDF of $\boldsymbol{\theta}_t$ given all other updating parameters. Note that, $p(\mathbf{a}|\cdot), p\left(\sigma_{\theta_i}^2|\cdot\right)$ and $p\left(\sigma_{e_j}^2|\cdot\right)$ are standard distributions and therefore can be sampled easily. $p(\boldsymbol{\theta}_t|\cdot)$ and $p(\mathbf{b}|\cdot)$ are only known up to a normalizing constant and need Markov Chain Monte Carlo (MCMC) methods to sample. Metropolis-Hastings (MH) algorithm [39,40] is chosen for sampling these two marginal distributions and the whole sampling approach is referred to as the MH within Gibbs sampling method.

Gibbs method samples the updating parameters one by one in a loop, and a complete loop generates one sample for all the updating parameters. Furthermore, this is often a high-dimensional problem and requires a large number of samples to converge. Therefore, it is computationally prohibitive to directly use the proposed MH within Gibbs sampling approach to generate an adequate number of samples to provide accurate statistics of the updating parameters, e.g., maximum a posteriori (MAP), mean and standard deviation. Instead, a simplified approach for MAP estimations is proposed here [29]. This approach is described below:

(1) Initial guess for MAP estimates: ${}^0\hat{\mathbf{a}}, {}^0\hat{\mathbf{b}}, {}^0\hat{\boldsymbol{\Sigma}}_{\boldsymbol{\theta}}, {}^0\hat{\boldsymbol{\Sigma}}_{\mathbf{e}}$

(2) At iteration k

(a) Compute ${}^k\hat{\boldsymbol{\theta}}_t$ given ${}^{k-1}\hat{\mathbf{a}}, {}^{k-1}\hat{\mathbf{b}}, {}^{k-1}\hat{\boldsymbol{\Sigma}}_{\boldsymbol{\theta}}, {}^{k-1}\hat{\boldsymbol{\Sigma}}_{\mathbf{e}}$

$${}^k\hat{\boldsymbol{\theta}}_t = \arg\min_{\boldsymbol{\theta}_t}(J_{\mathbf{e}_t} + J_{\boldsymbol{\theta}_t}) \tag{23}$$

(b) Compute MAP of $\mathbf{a}$ and $\mathbf{b}$ given ${}^k\hat{\boldsymbol{\theta}}_t, {}^{k-1}\hat{\boldsymbol{\Sigma}}_{\boldsymbol{\theta}}$

$$\left({}^k\hat{\mathbf{a}}, {}^k\hat{\mathbf{b}}\right) = \arg\min_{\mathbf{a},\mathbf{b}}\left(\sum_{t=1}^{N_t} J_{\boldsymbol{\theta}_t}\right) \tag{24}$$

(c) Find MAP of $\boldsymbol{\Sigma}_{\boldsymbol{\theta}}, \boldsymbol{\Sigma}_{\mathbf{e}}$

$${}^k\hat{\sigma}_{\theta_i}^2 = \frac{\nu_1\sigma_{\theta 0_i}^2 + N_t S_i}{\nu_1 + N_t + 2} \tag{25}$$

$${}^k\hat{\sigma}_{e_j}^2 = \frac{\nu_2\sigma_{e0_j}^2 + N_t V_j}{\nu_2 + N_t + 2} \tag{26}$$

(3) Repeat step (2) until convergence criteria is reached

This simplified approach is adequate to find the MAPs of the updating parameters. However, in order to estimate the parameters' uncertainties, the standard MH within Gibbs sampler can be employed by using the estimated MAPs as the starting point to reach faster convergence of sampled parameters. This two-step sampling approach is capable of providing MAPs and estimation uncertainty of the updating parameters with less computation effort.

5. Application to the two-story RC building

5.1. Initial FE model

A linear FE model of the structure is built in the open-source FE analysis software OpenSees [41]. OpenSees is convenient for model updating applications as it is computationally efficient in analysis and flexible to be linked to other programs such as Matlab where the sampling is performed. A lidar scanner was used to collect and create the point cloud of the building [15], and the geometry of the model is estimated from the lidar data. Concrete and masonry samples were extracted from the building for columns, slabs and walls, and then sent to University of California San Diego Structural Engineering Powell Laboratory for material property test [30]. Young's modulus of columns and masonry walls in the initial model are based on the lab test results of the extracted samples. The RC frames of the structure are modeled using linear elastic beam-column elements. The floor slabs are assumed to be rigid in-plane based on the fact that the slabs are strong in-plane due to its geometry and material properties. This assumption is checked using the mode shape components (10 channels) on each floor and the corresponding shapes using a fitted least-squares rigid body motion. The assumption is found to be reasonable in the view of identification errors. The masonry walls of the building are modeled as diagonal struts, with their cross-section and stiffness estimated based on FEMA 356 [42]. The equivalent struts have the same thickness and Young's modulus as the masonry wall, and their widths are estimated from:

$$a = 0.175(\lambda_l h_{col})^{-0.4} r_{inf} \tag{27}$$

where λ_l denotes the coefficient of strut width which is determined by the geometry and stiffness of the infills and frames, h_{col} is the height of side columns, and r_{inf} refers to the diagonal length of the infill panel. The foundation of the building is modeled as fixed and soil-structure interaction is not considered. The structural mass is estimated based on the densities of extracted samples and the geometry from lidar data and is assigned as lumped mass at the nodes of the FE model. This linear FE model is considered as the initial model in the hierarchical Bayesian model updating framework with the stiffness of considered substructures varying as a function of the vibration level.

5.2. Model updating results

The proposed hierarchical Bayesian model updating approach is applied using the available 41 datasets of identified modal parameters at different excitation amplitudes. Based on the sensitivity study performed, five stiffness parameters are selected for updating with each representing a substructure of the building, $\boldsymbol{\theta} = [\theta_1, \cdots, \theta_5]^T$. The stiffness parameters are defined as the normalized Young's modulus $\theta_i = E_i/E_i^0$. E_i denotes the Young's modulus of substructure i and E_i^0 is the initial value. The five substructures include: all the infill walls at the west side of the 2nd story (θ_1), east walls of the 2nd story (θ_2), north walls of the 2nd story (θ_3), south walls of the 2nd story (θ_4), and all walls of the 1st story and all columns (θ_5). Note that initial damage and evident cracks were observed in the infill walls of the second story and therefore four of the updating parameters are selected at this story to characterize the uncertain stiffness of damaged infills.

The estimated MAP values of hyperparameters and covariance of error function using the simplified approach are summarized in Table 2. Note that the reported $\hat{\sigma}_e$ for mode shapes 1 ($\boldsymbol{\Phi}_1$) and 2 ($\boldsymbol{\Phi}_2$) refer to the average values over all mode shape components. $\hat{\mathbf{a}}$ can be interpreted as the mean of the stiffness parameters at zero vibration level. It can be observed that there is a large discrepancy among values of $\hat{\mathbf{a}}$ for different substructures which is due to the different levels of existing damage in the building. Evident cracks were observed in the west (θ_1), north (θ_3) and south walls (θ_4) of the 2nd story, corresponding to the small values of $\hat{\mathbf{a}}$. The fact that the values of $\hat{\mathbf{a}}$ (θ_1, θ_3) are close to zero indicates the west and north walls of 2nd story are severely damaged and barely provide any stiffness. These values are consistent with the observed damage at the 2nd story of the building [15]. The east walls of 2nd story (θ_2) are relatively intact, so $\hat{\mathbf{a}}$ (θ_2) is close to 1. $\hat{\mathbf{a}}$ (θ_5) shows a significant increase which means the stiffness of columns and walls of the 1st story were underestimated in the initial FE model, probably due to the effects of modeling errors such as use of diagonal struts for masonry walls. The estimated components of $\hat{\mathbf{b}}$ are negative indicating that the stiffness of all substructures decrease with higher vibration level, which is consistent with the observed decreasing trend of natural frequencies in Fig. 5. The decreasing trend of natural frequencies with high vibration level is due to the crack opening/closing of the building. This linear decreasing trend is accounted for and

Table 2
MAPs of updating parameters from simplified approach.

	$\hat{\mathbf{a}}$	$\hat{\mathbf{b}}$	$\hat{\sigma}_\theta$		$\hat{\sigma}_e(\%)$
(θ_1)	0.11	−2.41	0.011	(λ_1)	0.02
(θ_2)	0.85	−4.68	0.008	(λ_2)	0.98
(θ_3)	0.08	−0.44	0.010	($\boldsymbol{\Phi}_1$)	1.32
(θ_4)	0.40	−4.91	0.017	($\boldsymbol{\Phi}_2$)	1.98
(θ_5)	1.82	−22.66	0.065		

quantified by the parameter $\hat{\mathbf{b}}$. It can be observed that the value of $\hat{\mathbf{b}}$ for θ_5 is much larger than that of θ_1 to θ_4. This can be due to the fact that θ_5 contains the least damaged components of the structure and its stiffness can be affected more significantly from crack openings than other already severely damaged substructures. Note that the values of $\hat{\mathbf{a}}$ and $\hat{\mathbf{b}}$ are only valid and meaningful within the range of observed vibration levels, i.e., 0–0.045 m/s^2 and the assumed linear function of $\boldsymbol{\mu}_{\boldsymbol{\theta}}$ should not be extrapolated for much larger amplitudes since that may result in negative structural stiffness. The uncertainties in the updated stiffness parameters are quantified by $\hat{\sigma}_\theta$, with the largest uncertainty estimated for θ_5, however the estimated uncertainties are relatively small compared to the values of $\hat{\mathbf{a}}$. From the table, it is also seen that the error functions have small uncertainties ($\hat{\sigma}_e$), with relatively larger standard deviations for mode 2 (both in eigen-frequency and mode shape).

Using the proposed two-step sampling approach, samples of the updating parameters are generated using the MH within Gibbs sampler after the MAPs are estimated. 1000 samples are generated and histograms of the samples for a_i, b_i and σ_{θ_i} are shown in Fig. 7. Note that some of the stiffness components (especially θ_1) get close to zero at high vibration levels. Therefore, to avoid having negative stiffness and instability, all stiffness samples are truncated to be positive. Although this truncation would violate the normal distribution assumption, negative stiffness is only obtained at very high vibration levels and only for θ_1, therefore its effect is negligible. Alternatively, other distribution models can be used to avoid this issue. From Fig. 7, it can be seen that samples of a_i and b_i approximately follow a normal distribution. Samples of σ_{θ_i} seem to follow the Inverse $-\chi^2$ distribution with a tail on the right side due to the conjugate priors used. Overall, the uncertainties of all hyperparameters are small and these uncertainties decrease as more informative datasets are considered. While the estimation uncertainties of hyperparameter can be reduced by feeding more measured data into the framework, the MAP values tend to stay constant and will not be affected by using more data (once adequate data is available). Therefore, the estimated uncertainties of structural stiffness and modeling errors will not change significantly by increasing the amount of data in the implemented framework. On the contrary, such estimation uncertainties of structural stiffness will not converge and will consistently decrease with the addition of data in the traditional Bayesian inference formulation [29].

5.3. Probabilistic response prediction

5.3.1. Modal parameter prediction

Using the updated model, response or response features of the building such as its modal parameters can be predicted at different levels of vibration amplitude. The predicted modal parameters can be used to verify the accuracy and performance of the proposed hierarchical Bayesian framework. Model-predicted modal parameters can be evaluated by transforming the definition of error function in Eqs. (4) and (5) into the following:

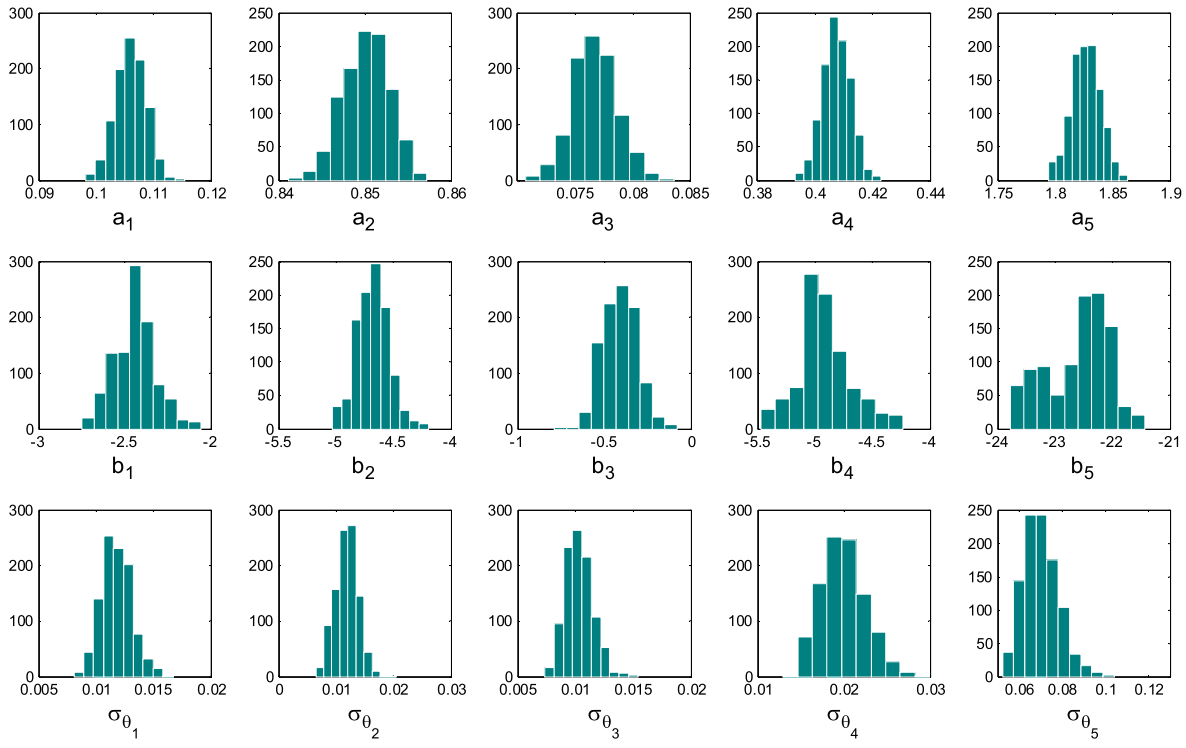

Fig. 7. Histograms of 1000 samples of hyperparameters generated using MH within Gibbs.

$$\lambda_{tm}^{\text{pre}} = \lambda_m(\boldsymbol{\theta}_t) + \lambda_m(\boldsymbol{\theta}_t) e_{\lambda_{tm}} \tag{28}$$

$$\frac{\boldsymbol{\Phi}_{tm}^{\text{pre}}}{\left\|\boldsymbol{\Phi}_{tm}^{\text{pre}}\right\|} = \left(\frac{\boldsymbol{\Gamma}\boldsymbol{\Phi}_m(\boldsymbol{\theta}_t)}{\|\boldsymbol{\Gamma}\boldsymbol{\Phi}_m(\boldsymbol{\theta}_t)\|} + \mathbf{e}_{\boldsymbol{\Phi}_{tm}}\right) \Big/ \left\| \frac{\boldsymbol{\Gamma}\boldsymbol{\Phi}_m(\boldsymbol{\theta}_t)}{\|\boldsymbol{\Gamma}\boldsymbol{\Phi}_m(\boldsymbol{\theta}_t)\|} + \mathbf{e}_{\boldsymbol{\Phi}_{tm}} \right\| \tag{29}$$

in which stiffness parameters $\boldsymbol{\theta}_t$ follow the normal distribution $\boldsymbol{\theta}_t \sim N(\hat{\mathbf{a}} + \hat{\mathbf{b}}\varepsilon_t, \hat{\boldsymbol{\Sigma}}_{\boldsymbol{\theta}})$. $e_{\lambda_{tm}}$ and $\mathbf{e}_{\boldsymbol{\Phi}_{tm}}$ denote the corresponding eigen-frequency error and mode shape error which follow the assumed zero-mean Gaussian distribution $\mathbf{e}_t \sim N(\mathbf{0}, \hat{\boldsymbol{\Sigma}}_{\mathbf{e}})$. Note that the predicted mode shapes $\boldsymbol{\Phi}_{tm}^{\text{pre}}$ are approximated solutions as the original error function is implicit with respect to $\tilde{\boldsymbol{\Phi}}_{tm}$ (due to a_{tm}). However, the approximation error should be negligible as the covariance matrix of error function is relatively small.

A total of 1000 samples of natural frequencies are predicted for the first two modes with vibration levels uniformly distributed in the range of test data. The predictions are compared with the identified natural frequencies in Fig. 8. It can be seen that the predictions follow the decreasing trend and cover the scattering range of the identified values very well. Both point clouds (gray circles and black dots) show similar uncertainties along the range of vibration level. Note that the drop in identified natural frequencies are most likely caused by crack openings in the building, and this phenomenon is correctly reproduced by the assumed function between stiffness and vibration level using the linear FE model. This demonstrates the effectiveness of the proposed hierarchical Bayesian framework to capture and reproduce the observed characteristics of modal parameters.

5.3.2. Time history response prediction

Accurate prediction of the dynamic time history response is one of the major goals of modeling and model updating of structural systems and is critical for evaluating structural performance under future loading. In this section, displacement and acceleration time histories of the building are predicted when subjected to a shaker excitation using the probabilistically calibrated model. The dynamic responses are estimated through modal superposition considering only the first two modes.

The equation of motion in modal coordinates [33] can be expressed as:

$$\ddot{q}_m(t) + 2\zeta_m\omega_m\dot{q}_m(t) + \omega_m^2 q_m(t) = \frac{P_m(t)}{M_m} \tag{30}$$

in which $q_m(t)$ is the modal displacement response at time t for mode m. ζ_m is the damping ratio, ω_m is the natural frequency in rad/s, $\omega_m = \sqrt{\lambda_{tm}^{\text{pre}}}$. $P_m(t)$ is the generalized force with $P_m(t) = \boldsymbol{\Phi}_m^T\mathbf{p}(t)$ where $\mathbf{p}(t)$ is the input force vector. M_m is the generalized mass, $M_m = \boldsymbol{\Phi}_m^T\mathbf{M}\Phi_m$. Once the modal response is predicted, it can be transformed into physical coordinates using the model-predicted mode shapes:

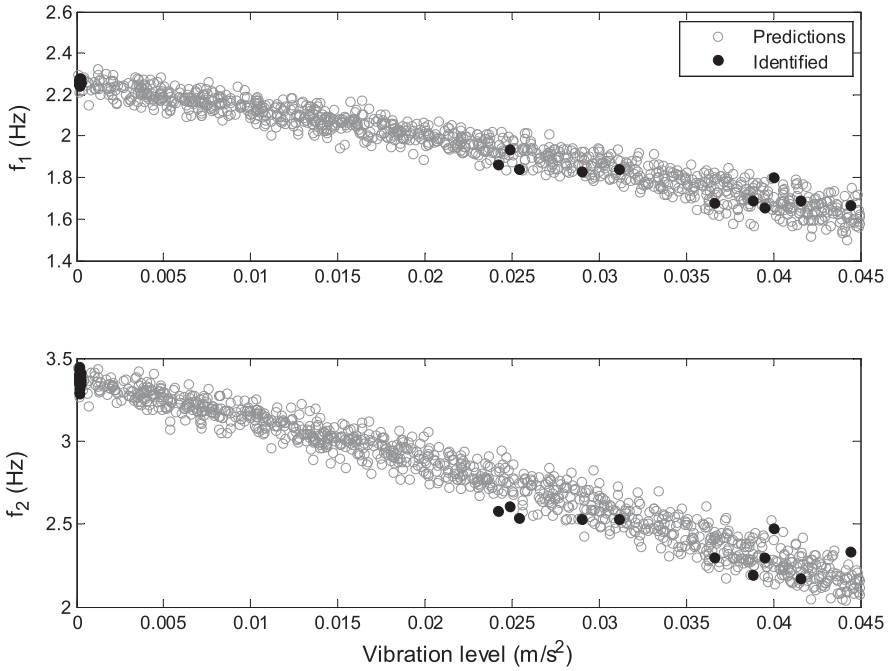

Fig. 8. Comparison of 1000 natural frequency predictions and their identified counterparts.

$$\mathbf{y}^{\text{pre}}(t) = \begin{bmatrix} \boldsymbol{\Phi}_1^{\text{pre}} & \boldsymbol{\Phi}_2^{\text{pre}} \end{bmatrix} \begin{bmatrix} q_1(t) \\ q_2(t) \end{bmatrix} \tag{31}$$

The velocity and acceleration responses can be estimated in a similar manner by replacing q_m with $\dot{q}_m$ or $\ddot{q}_m$ in Eq. (31). Note that the predicted mode shapes only contain components at the location of available sensors, therefore this formulation only provides predictions at degrees-of-freedom (DOFs) with available measurements. However, the error function can be expanded to provide predictions at all DOFs of the model. Two approaches can be used for expanding the error function: (1) using the largest components of $\hat{\sigma}_{e_j}$ for the unmeasured DOFs as it is done in the study [36] (this is a conservative approach), or (2) using $\hat{\sigma}_{e_j}$ of the closest measured DOF for unmeasured DOFs.

The acceleration response time history of the building is predicted when the building is subjected to a sine sweep excitation in Y direction. The input force of the shaker is not measured directly but it is estimated based on the excitation frequency measurement and the weight of the shaker [43]:

$$u(t) = A(t)\sin(\varphi(t)) \tag{32}$$

In Eq. (32), $A(t)$ is the shaker instant force and $A(t) = 2MR(2\pi f(t))^2$. MR denote the eccentricity which is the product of the eccentric mass and the distance between center of mass and center of shaft, and is equal to 652.38 kg-m. $f(t)$ is the measured instant input frequency in Hz and is shown in Fig. 9(a). $\varphi(t)$ is the phase of the shaker which can be evaluated through:

$$\varphi(t) = \varphi_0 + \int_0^t 2\pi f(t)dt \tag{33}$$

in which φ_0 is the initial phase of the shaft, and is estimated as $-\pi/4$ using the measured response at channel NW-X. The estimated shaker input force is shown in Fig. 9(b).

In the formulated hierarchical Bayesian framework, the mean of stiffness parameters $\boldsymbol{\mu}_{\boldsymbol{\theta}}(\varepsilon_t)$ depend on the vibration level ε_t. The vibration level ε_t can be estimated based on the excitation force using the transfer function of the calibrated model. The vibration level for the considered sine sweep excitation is evaluated to be 0.039 m/s^2 from the measured data. Damping is another factor that affects the time history response predictions. To account for the uncertainties of modal damping, the damping ratios are assumed to follow a normal distribution with mean and standard deviation the same as those identified from forced vibration tests (see Table 1), $\zeta_1(\%) \sim N\left(5.9, 1.1^2\right)$ and $\zeta_2(\%) \sim N\left(8.6, 1.2^2\right)$. Note that although the identified damping ratios of the first two modes increase significantly for forced vibrations, they do not follow a clear trend. Furthermore, the identified damping ratios usually have larger estimation uncertainty than the natural frequencies. Thus, accounting for the relationship between damping and amplitude is considered outside the scope of this study. This provides more conservative confidence intervals for the predictions.

A total of 100 independent acceleration response time history predictions are generated considering uncertainties of stiffness, error function and damping ratios. A 95% confidence interval of the time history predictions is estimated by: (1) sorting the 100 predictions at each time instant in an increasing order; (2) selecting the 4th and 98th values as the lower and upper bounds of the interval. Thus, the bounds do not correspond to complete individual realizations of response at tail values of parameters. The comparison between predicted acceleration time histories and the measured data for the sensors on the roof is shown in Fig. 10. It can be seen that the predictions have a good agreement with the measured data and measurements fall within the 95% confidence intervals. The predictions are capable of predicting the peaks of the measured data very well, with the peak amplitude slightly larger than the measured data due to the uncertainties considered in the predictions. The confidence bounds for some channels are tighter than others, e.g., bounds for channels NW-X and NE-X are tighter than channel NE-Y and SW-Y. However, some discrepancies can be observed, e.g., the central peak of NW-X measured data around 120 s

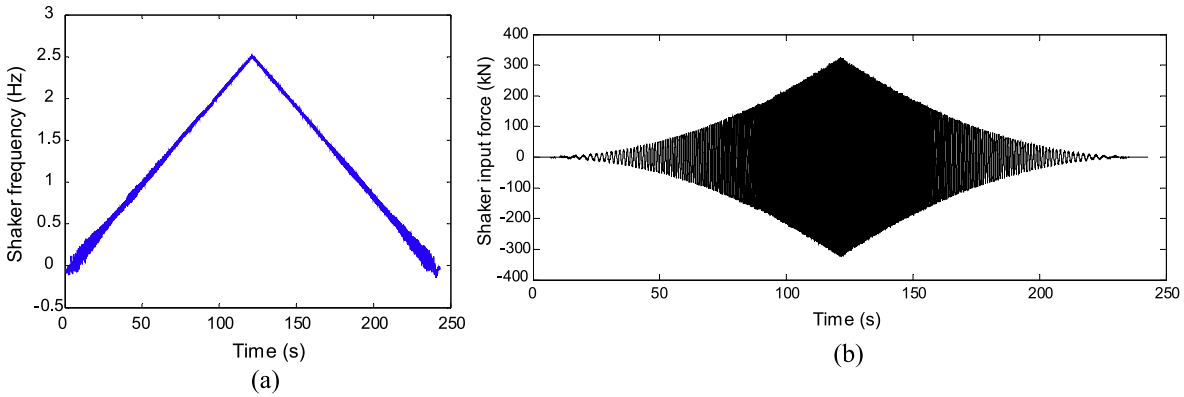

Fig. 9. (a) Shaker excitation frequency; (b) Estimated shaker input force.

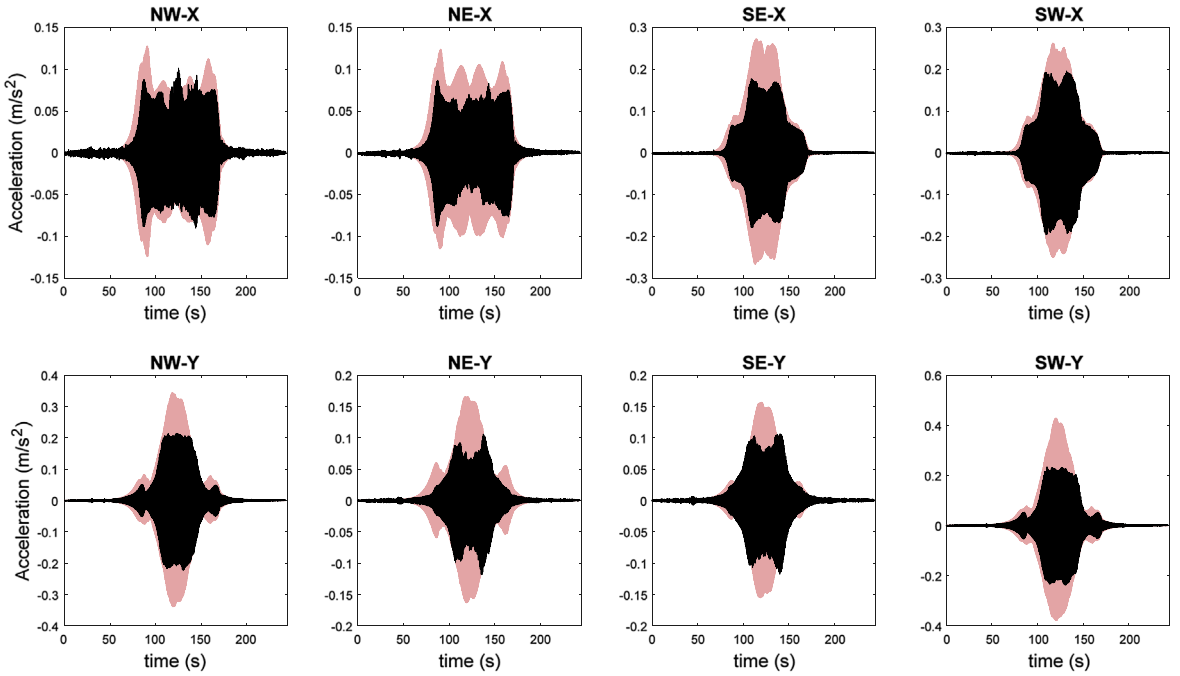

Fig. 10. Comparison of predicted acceleration time histories and measured data for sensors on the roof (light pink area refers to 95% confidence interval and black line denotes the measured data). (For interpretation of the references to colour in this figure legend, the reader is referred to the web version of this article.)

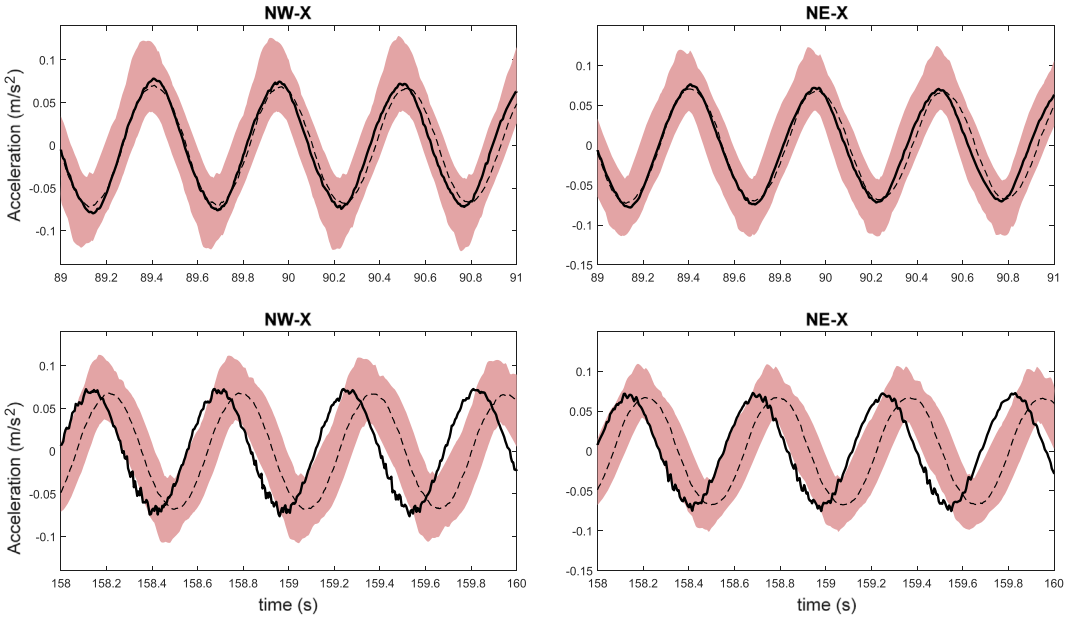

Fig. 11. Zoom-in plot (89–91 s for top two graphs, and 158–160 s for bottom two graphs) of the acceleration comparison for channels NW-X and NE-X (light pink area refers to 95% confidence interval, dashed line refers to the median of predictions, and black line denotes the measured data). (For interpretation of the references to colour in this figure legend, the reader is referred to the web version of this article.)

which is due to the fact that in the implemented framework, a constant vibration level is defined for the whole sine sweep shaker test while the excitation amplitude (and therefore the natural frequency) varies continuously during the test. The zoom-in plot of the comparison for the peak amplitude between 89–91 s and 158–160 s for channels NW-X and NE-X is shown in Fig. 11. It can be observed that the measured data falls within the light pink area which represents the 95% con-

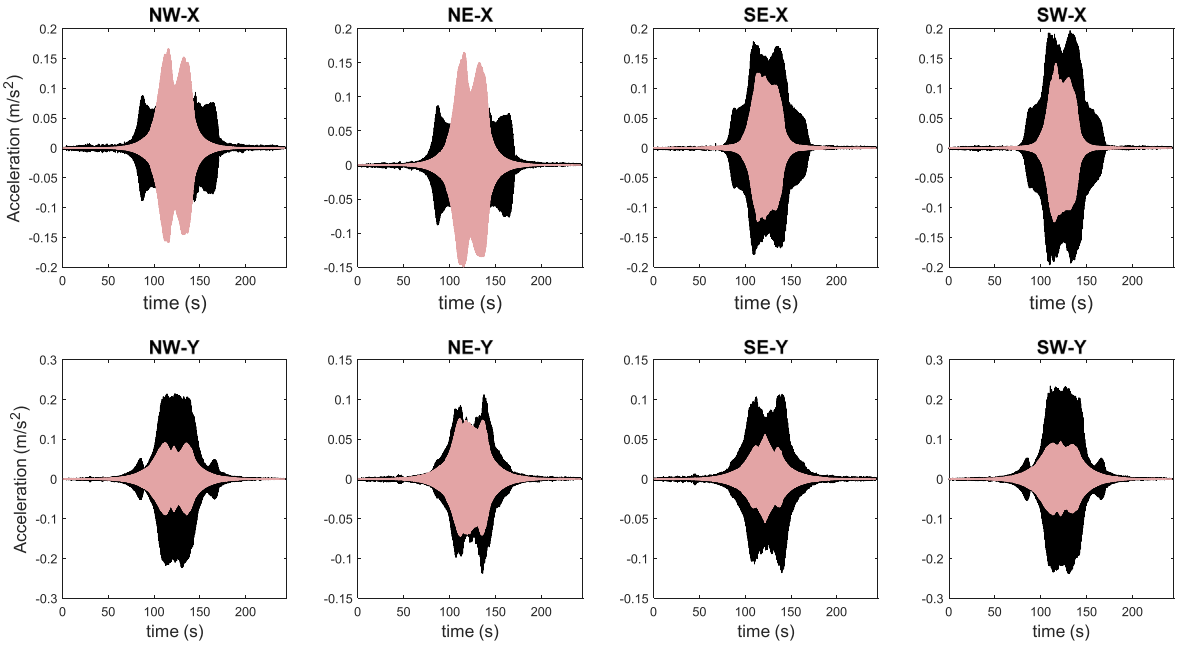

Fig. 12. Comparison of predicted acceleration time histories using ambient vibration level and the measured data for sensors on the roof (light pink area refers to 95% confidence interval and black line denotes the measured data). (For interpretation of the references to colour in this figure legend, the reader is referred to the web version of this article.)

fidence interval for window 89–91 s (top two graphs in Fig. 11), but there is a small time offset between measured and predictions for window 158–160 s (bottom two graphs in Fig. 11) which is due to the fact that a small change in natural frequency would accumulate the phase shift of the response. However, response amplitude is always within the prediction interval if the time shift is corrected. The predictions can be improved by allowing the stiffness to change continuously with the vibration level in a single excitation test which would demand a higher computational cost but it is feasible to do so.

To underline the importance of accounting for vibration amplitude in model updating and response prediction, the time history response are predicted again from the calibrated model without considering the stiffness-amplitude dependence, i.e., the calibrated model at ambient vibration level is used for predicting response to the same shaker excitation. The same modal superposition procedure and damping ratio distributions are applied. Similar comparison of predicted acceleration time histories with the measured data for the roof sensors is shown in Fig. 12. It can be seen that the model cannot predict the peaks of the measured data and the confidence bounds do not contain the measurements. This demonstrates that for the considered damaged building, a model calibrated using ambient data is not suitable for predicting the structural response at higher vibration level. It also highlights the capability of a hierarchical Bayesian framework for considering and modeling different sources of uncertainty/variability such as the stiffness versus excitation amplitude.

6. Summary and conclusions

This paper presents a hierarchical Bayesian model updating framework which accounts for the effects of excitation amplitude on structural stiffness. The approach has been implemented for model calibration and dynamic response prediction of a two-story RC building that was severely damaged due to past earthquakes. Modal parameters of the structure are identified using both ambient and forced vibration data, and the identified natural frequencies are observed to decrease significantly at higher vibration level. The hierarchical Bayesian model updating approach is applied to estimate the stiffness parameters of five considered substructures, stiffness hyperparameters (mean and covariance of stiffness parameters), as well as modeling errors. To account for stiffness-amplitude dependence, stiffness mean is assumed to have a linear relationship with the vibration level, and stiffness covariance is assumed to be constant. The joint posterior PDF of all updating parameters (stiffness parameters, stiffness mean which is a function of vibration level, stiffness covariance, and covariance of error function) is derived from likelihood functions and prior PDFs given measured data. A two-step sampling approach is proposed to first compute the MAPs of the updating parameters, and then evaluate their estimation uncertainties using MH within Gibbs sampler. Time history responses of the building are finally predicted when the building is subjected to a high amplitude sine-sweep shaker excitation and compared with the measured data.

The proposed hierarchical Bayesian model updating framework has successfully provided the following results:

(I) *Most probable values and estimation uncertainties of all updating parameters*: the MAPs of all updating parameters and their estimation uncertainties are successfully estimated through the proposed two-step sampling approach, including effective stiffness in each dataset, stiffness mean (as a function of vibration level) and covariance, and covariance of error function. Based on the MAP results, stiffness of the west, north and south walls of 2nd story need to be reduced significantly, indicating the extent of damage at these locations.

(II) *Inherent uncertainty of stiffness parameters*: the inherent uncertainty of stiffness parameters due to ambient and environmental conditions such as changing temperature and wind excitation is quantified by the stiffness hyperparameters (stiffness mean and covariance). While the estimation uncertainties of hyperparameter can be reduced by feeding more data into the framework, the MAP values such as the stiffness covariance converge. Such convergence cannot be achieved in alternative Bayesian inference formulations.

(III) *Modeling errors estimation:* modeling errors are approximately quantified through the assumed normal distribution of error function which is characterized by its mean and covariance (no modeling bias is considered, but could be estimated in this framework as shown in the study [36]), which are then considered and propagated in the natural frequency and time history response predictions.

(IV) *Stiffness versus excitation amplitude relationship within the updating framework*: the proposed framework provides the MAPs and estimation uncertainties of the considered underlying relationship between stiffness mean and vibration level. Accounting for this major source of variability in the dynamic behavior of the building reduces the uncertainty of stiffness parameters (a much larger stiffness covariance will be estimated if the stiffness-amplitude relationship is removed), and therefore provides tighter confidence bounds for time history response predictions.

Acknowledgement

The authors acknowledge partial support of this study by the National Science Foundation Grant number 1254338 as well as Grant number 1430180 that supported vibration testing of the considered building. The authors would like to thank Dr. Seyedsina Yousefianmoghadam and Dr. Supratik Bose for their guidance in modeling of the building in OpenSees. Dr. Seyedsina Yousefianmoghadam was leading the in situ dynamic test of the building and his great effort and contribution to this project is gratefully acknowledged. The opinions, findings, and conclusions expressed in this paper are those of the authors and do not necessarily represent the views of the sponsors and organizations involved in this project.

References

[1] J.E. Mottershead, M. Friswell, Model updating in structural dynamics: a survey, J. Sound Vib. 167 (1993) 347–375.
[2] M. Friswell, J.E. Mottershead, Finite Element Model Updating in Structural Dynamics, Springer Science & Business Media, 2013.
[3] J.M. Brownjohn, P.-Q. Xia, Dynamic assessment of curved cable-stayed bridge by model updating, J. Struct. Eng. 126 (2000) 252–260.
[4] J.M.W. Brownjohn, P. Moyo, P. Omenzetter, et al, Assessment of highway bridge upgrading by dynamic testing and finite-element model updating, J. Bridge Eng. 8 (2003) 162–172.
[5] Q. Zhang, T.-Y.P. Chang, C.C. Chang, Finite-element model updating for the Kap Shui Mun cable-stayed bridge, J. Bridge Eng. 6 (2001) 285–293.
[6] A. Teughels, G. De Roeck, Structural damage identification of the highway bridge Z24 by FE model updating, J. Sound Vib. 278 (2004) 589–610.
[7] B. Jaishi, H.-J. Kim, M.K. Kim, et al, Finite element model updating of concrete-filled steel tubular arch bridge under operational condition using modal flexibility, Mech. Syst. Sig. Process. 21 (2007) 2406–2426.
[8] B. Jaishi, W.-X. Ren, Finite element model updating based on eigenvalue and strain energy residuals using multiobjective optimisation technique, Mech. Syst. Sig. Process. 21 (2007) 2295–2317.
[9] E. Reynders, G.D. Roeck, P. Gundes Bakir, et al, Damage identification on the Tilff Bridge by vibration monitoring using optical fiber strain sensors, J. Eng. Mech. 133 (2007) 185–193.
[10] R. Perera, A. Ruiz, A multistage FE updating procedure for damage identification in large-scale structures based on multiobjective evolutionary optimization, Mech. Syst. Sig. Process. 22 (2008) 970–991.
[11] B. Moaveni, I. Behmanesh, Effects of changing ambient temperature on finite element model updating of the Dowling Hall Footbridge, Eng. Struct. 43 (2012) 58–68.
[12] S.-E. Fang, R. Perera, G. De Roeck, Damage identification of a reinforced concrete frame by finite element model updating using damage parameterization, J. Sound Vib. 313 (2008) 544–559.
[13] B. Moaveni, X. He, J.P. Conte, et al, Damage identification study of a seven-story full-scale building slice tested on the UCSD-NEES shake table, Struct. Saf. 32 (2010) 347–356.
[14] B. Moaveni, A. Stavridis, G. Lombaert, et al, Finite-element model updating for assessment of progressive damage in a 3-story infilled RC frame, J. Struct. Eng. 139 (2012) 1665–1674.
[15] M. Song, S. Yousefianmoghadam, M.-E. Mohammadi, et al, An application of finite element model updating for damage assessment of a two-story reinforced concrete building and comparison with lidar, Struct. Health Monit. (2017), 1475921717737970.
[16] E. Bassoli, L. Vincenzi, A.M. D'Altri, et al, Ambient vibration-based finite element model updating of an earthquake-damaged masonry tower, Struct. Control Health Monit. 25 (2018) e2150.
[17] B. Moaveni, J.P. Conte, F.M. Hemez, Uncertainty and sensitivity analysis of damage identification results obtained using finite element model updating, Comput.-Aided Civ. Infrastruct. Eng. 24 (2009) 320–334.
[18] J.L. Beck, L.S. Katafygiotis, Updating models and their uncertainties. I: Bayesian statistical framework, J. Eng. Mech. 124 (1998) 455–461.
[19] L.S. Katafygiotis, J.L. Beck, Updating models and their uncertainties. II: model identifiability, J. Eng. Mech. 124 (1998) 463–467.
[20] H. Sohn, K.H. Law, A Bayesian probabilistic approach for structure damage detection, Earthquake Eng. Struct. Dyn. 26 (1997) 1259–1281.
[21] J. Ching, J.L. Beck, New Bayesian model updating algorithm applied to a structural health monitoring benchmark, Struct. Health Monit. 3 (2004) 313–332.

[22] K.V. Yuen, J.L. Beck, S.K. Au, Structural damage detection and assessment by adaptive Markov chain Monte Carlo simulation, Struct. Control Health Monit. 11 (2004) 327–347.
[23] M. Muto, J.L. Beck, Bayesian updating and model class selection for hysteretic structural models using stochastic simulation, J. Vib. Control 14 (2008) 7–34.
[24] E. Ntotsios, C. Papadimitriou, P. Panetsos, et al, Bridge health monitoring system based on vibration measurements, Bull. Earthq. Eng. 7 (2009) 469.
[25] H.F. Lam, J.H. Yang, S.K. Au, Markov chain Monte Carlo-based Bayesian method for structural model updating and damage detection, Struct. Control Health Monit. 25 (2018) e2140.
[26] I. Behmanesh, B. Moaveni, Probabilistic identification of simulated damage on the Dowling Hall footbridge through Bayesian finite element model updating, Struct. Control Health Monit. 22 (2015) 463–483.
[27] I. Behmanesh, B. Moaveni, Accounting for environmental variability, modeling errors, and parameter estimation uncertainties in structural identification, J. Sound Vib. 374 (2016) 92–110.
[28] E. Asgarieh, B. Moaveni, A.R. Barbosa, et al, Nonlinear model calibration of a shear wall building using time and frequency data features, Mech. Syst. Sig. Process. 85 (2017) 236–251.
[29] I. Behmanesh, B. Moaveni, G. Lombaert, et al, Hierarchical Bayesian model updating for structural identification, Mech. Syst. Sig. Process. 64 (2015) 360–376.
[30] S. Yousefianmoghadam, Investigation of the Linear and Non-Linear Dynamic Behavior of actual RC Buildings through Tests and Simulations PhD Thesis, University at Buffalo, USA, 2019.
[31] G. James, T.G. Carne, J.P. Lauffer, The natural excitation technique (NExT) for modal parameter extraction from operating structures, Modal Anal.-the Int. J. Anal. Exp. Modal Anal. 10 (1995) 260.
[32] J.-N. Juang, R.S. Pappa, An eigensystem realization algorithm for modal parameter identification and model reduction, J. Guidance, Control, Dyn. 8 (1985) 620–627.
[33] A.K. Chopra, A.K. Chopra, Dynamics of Structures: Theory and Applications to Earthquake Engineering, Pearson/Prentice Hall Upper Saddle River, NJ, 2007.
[34] J.F. Clinton, S.C. Bradford, T.H. Heaton, et al, The observed wander of the natural frequencies in a structure, Bull. Seismol. Soc. Am. 96 (2006) 237–257.
[35] J.L. Beck, S.K. Au, M.W. Vanik, Monitoring structural health using a probabilistic measure, Comput.-Aided Civ. Infrastruct. Eng. 16 (2001) 1–11.
[36] M. Song, I. Behmanesh, B. Moaveni, Hierarchical, et al, Bayesian Calibration and Response Prediction of a 10-Story Building Model. *Model Validation and Uncertainty Quantification, Volume 3*, Springer (2019) 153–165.
[37] A. Gelman, H.S. Stern, J.B. Carlin, et al, Bayesian Data Analysis, Chapman and Hall/CRC, 2013.
[38] J. Kruschke, Doing Bayesian Data Analysis: A tutorial with R, JAGS, and Stan, Academic Press, 2014.
[39] N. Metropolis, A.W. Rosenbluth, M.N. Rosenbluth, et al, Equation of state calculations by fast computing machines, J. Chem. Phys. 21 (1953) 1087–1092.
[40] W.K. Hastings. Monte Carlo sampling methods using Markov chains and their applications. 1970.
[41] OpenSees 2.5.0. UC Berkeley.
[42] Council BSS. Prestandard and commentary for the seismic rehabilitation of buildings. Report FEMA-356, Washington, DC 2000.
[43] S. Orlando, B. Peeters, G. Coppotelli. Improved FRF estimators for MIMO Sine Sweep data. In: Proceedings of the ISMA 2008 International Conference on Noise and Vibration Engineering 2008, 229–241.